Pineapple Lectin AcmJRL Binds SARS-CoV-2 Spike Protein in a Carbohydrate-Dependent Fashion**

Joscha Meiers+,[a, b, c] Jan Dastbaz+,[b, d, e] Sebastian Adam,[b, f] Sari Rasheed,[b, d, e] Susanne H. Kirsch,[b, e] Peter Meiser,[g] Peter Gross,*[h] Rolf Müller,*[b, d, e] and Alexander Titz*[a, b, c]

The highly glycosylated spike protein of SARS-CoV-2 is essential for infection and constitutes a prime target for antiviral agents and vaccines. The pineapple-derived jacalin-related lectin AcmJRL is present in the medication bromelain in significant quantities and has previously been described to bind manno-sides. Here, we performed a large ligand screening of AcmJRL by glycan array analysis, quantified the interaction with carbohydrates and validated high-mannose glycans as preferred ligands. Because the SARS-CoV-2 spike protein was previously reported to carry a high proportion of high-mannose N-glycans, we tested the binding of AcmJRL to the recombinantly produced extraviral domain of spike protein. We could demonstrate that AcmJRL binds the spike protein with a low-micro-molar K_D in a carbohydrate-dependent fashion.

Introduction

Since the end of 2019, the world has been facing the severe acute respiratory syndrome corona virus 2 (SARS-CoV-2) pandemic. SARS-CoV-2 is a novel coronavirus that has rapidly spread all over the world and is confirmed to have infected over 580 million people so far (August 2022, Johns Hopkins University). It infects the respiratory tract and potentially results in the coronavirus-associated disease COVID-19. Especially for older or immunocompromised patients, COVID-19 is likely to be lethal. So far, more than 6.3 million deaths have been reported in association with SARS-CoV-2.

A variety of novel and very potent vaccines entered the market at the end of 2020. Vaccination is an indispensable approach to protect society from SARS-CoV-2 infection. However, a rising fraction of vaccinated individuals suffer from severe syndromes after infection due to a continuous adaptation of the virus. Furthermore, a very small fraction of people cannot be vaccinated due to medical preconditions.[1] Currently, first antiviral drugs like Remdesivir and Ritonavir/Nirmatrelvir (Paxlovid) are getting established in SARS-CoV-2 therapy and more are under investigation since we need novel pharmaceutical therapies to cure or prevent infections with SARS-CoV-2. Interestingly, for the currently used antivirals Paxlovid and Molnupiravir rebound infections have been reported, showing their possible limitations.[2]

Coronavirus spike proteins (S-proteins) are essential for the infection process, they are trimerising fusion proteins that consist of the two subunits S1 and S2. It has been shown that S-proteins have a complex and extensive glycosylation pattern,[3–6] and coronavirus spike proteins typically contain between 23 and 38 N-glycosylation sites[7] per protomer with a significant population of oligomannose-type glycans (28%).[3] The elucidation of the glycosylation pattern[7] of the SARS-CoV-2 S-protein has been essential for the development of an effective vaccine.[8] A site-specific glycan analysis by mass spectrometry

[a] Dr. J. Meiers,+ Prof. Dr. A. Titz
     Chemical Biology of Carbohydrates (CBCH)
     Helmholtz Institute for Pharmaceutical Research Saarland (HIPS)
     Helmholtz Centre for Infection Research
     66123 Saarbrücken (Germany)
     E-mail: alexander.titz@helmholtz-hips.de
[b] Dr. J. Meiers,+ J. Dastbaz,+ Dr. S. Adam, S. Rasheed, Dr. S. H. Kirsch,
     Prof. Dr. R. Müller, Prof. Dr. A. Titz
     Deutsches Zentrum für Infektionsforschung (DZIF)
     Standort Hannover-Braunschweig
     38124 Braunschweig (Germany)
[c] Dr. J. Meiers,+ Prof. Dr. A. Titz
     Department of Chemistry, Saarland University
     66123 Saarbrücken (Germany)
[d] J. Dastbaz,+ S. Rasheed, Prof. Dr. R. Müller
     Department of Pharmacy, Saarland University
     66123 Saarbrücken (Germany)
[e] J. Dastbaz,+ S. Rasheed, Dr. S. H. Kirsch, Prof. Dr. R. Müller
     Microbial Natural Products (MINS)
     Helmholtz Institute for Pharmaceutical Research Saarland (HIPS)
     Helmholtz Centre for Infection Research
     66123 Saarbrücken (Germany)
     E-mail: rolf.mueller@helmholtz-hips.de

[f] Dr. S. Adam
     Drug Design and Optimisation (DDOP)
     Helmholtz Institute for Pharmaceutical Research Saarland (HIPS)
     Helmholtz Centre for Infection Research
     66123 Saarbrücken (Germany)
[g] Dr. P. Meiser
     URSAPHARM Arzneimittel GmbH
     66129 Saarbrücken (Germany)
[h] Prof. Dr. P. Gross
     Hochschule Kaiserslautern, Protein Chemistry Group
     66953 Pirmasens (Germany)
     E-mail: peter.gross-ALP@hs-kl.de
[+] These authors contributed equally to this work.
[**] A previous version of this manuscript has been deposited on a preprint server (https://doi.org/10.1101/2022.05.27.493400).

ChemBioChem

Research Article
doi.org/10.1002/cbic.202200463

Chemistry Europe
European Chemical
Societies Publishing

has revealed that the 22 *N*-glycosylation sites on the S-protein monomer are occupied with a mixture of oligomannose-type, hybrid-type and complex-type glycans. The content of exclusively oligomannose-type glycosylation sites was determined to be 28%, which is above the level of typical host glycoproteins.[7] However, it is less than for other viral glycoproteins like HIV-1 Env, where the amount of oligomannose-type glycans was found to be around 60%.[7] *N*-glycosylation is not only vital for protein folding during protein expression, but glycans also shield antigenic epitopes of S-protein and allow the virus to evade the host's immune system.[9] Further, glycans are important ligands for the first interaction with the host through its cell-surface attachment receptors.[9] For viral entry in airway epithelial cells, the receptor-binding domain (RBD) of SARS-CoV-2 S-protein binds angiotensin-converting-enzyme-2 (ACE2) with high affinity.[10]

Given the extensive glycosylation of the S-proteins of coronaviruses, it has been hypothesised that targeting surface glycans of S-proteins could lead to a decreased virulence of SARS-CoV-2. In fact, a study revolving around 33 different plant carbohydrate-binding proteins, that is, lectins, observed antiviral activity for 15 plant lectins against SARS-CoV and feline infectious peritonitis virus (FIPV).[11] Interestingly, the most prominent antiviral properties were found for mannose-specific lectins, which might be related to oligomannose-type glycans being essential for S-protein function. Further, Hoffmann et al. and Stravalaci et al. showed the ability of mammalian lectins (e.g., CLEC4G, MBL) to block SARS-CoV-2 infection in vitro.[12,13]

Drug repurposing is a particularly interesting approach due to the acute nature of the current pandemic and has led to the use of Remdesivir. Bromelain, a pineapple (*Ananas comosus*) stem extract, is an approved drug that shows anti-edematous, anti-inflammatory and fibrinolytic properties and is thus used to cure trauma-induced swelling.[14,15] Proteases, peptidic protease inhibitors and the mannose-binding lectin AcmJRL (also called AnLec) are the three main protein components of bromelain.[16] It is likely that proteases are responsible for the anti-inflammatory properties of bromelain. Additionally, protease inhibitors prevent unspecific proteolysis as a safety mechanism that is slowly removed during the intake of bromelain. It was shown that bromelain can reduce SARS-CoV-2 infection of VeroE6 and Calu-3 cells in vitro.[17] A putative mode of action of AcmJRL remains to be uncovered.

AcmJRL was recently characterised by Azarkan et al.[18] and its surprisingly high content in bromelain was determined by Gross et al.[16] AcmJRL belongs to the family of jacalin-related lectins (JRL),[19] that are closely related to jacalin, the lectin isolated from jackfruit (*Artocarpus integrifolia*). The JRL family can be divided in two main classes according to their ligand specificity.[19] Galactose-specific JRL (gJRL) are found almost exclusively in the *Moraceae* plant family, most typically in the seed. Structurally, those JRLs are tetramers of four identical protomers, each containing one carbohydrate binding site. On the other hand, mannose-specific jacalin-related lectins (mJRL) are found in various plants. The structure of mannose-specific JRLs usually consists of two, four or eight unprocessed peptides. Isothermal titration calorimetry experiments with AcmJRL

revealed rather low binding affinity towards ᴅ-mannose, *N*-acetyl-glucosamine, and ᴅ-glucose, in descending order.[18] On the other hand, oligomannose structures like mannotriose (Man-α-1,6(Man-α-1,3)Man) and mannopentaose (Man-α-1,6(Man-α-1,3)Man-α-1,6(Man-α-1,3)Man) showed significantly higher binding.

Like other mannose-specific JRLs, AcmJRL adopts a characteristic β-prism fold and two monomers align side-by-side forming a dimer. Although a tetrameric form of AcmJRL could also be assigned from the monomers in the asymmetric unit, this is likely a crystallisation artefact (see below). In co-crystal structures with ᴅ-mannose and methyl α-ᴅ-mannopyranoside, two carbohydrates are bound by one monomer in a conserved binding pose. Overall, the interactions are comparable to the binding of ᴅ-mannose by BanLec, a closely related mannose-specific JRL from banana (*Musa acuminata*). BanLec is reported as a potent viral entry inhibitor of HIV-1, HCV and influenza virus.[20,21] However, the mitogenic activity of native BanLec limits its therapeutic use. Interestingly, the structure of AcmJRL shares similarities with a genetically engineered BanLec[21] with reduced mitogenic activity. Thus, Azarkan et al. postulated a potential use of AcmJRL as an alternative to BanLec against mannosylated viruses.

Here, the ligand specificity of AcmJRL was further characterised by two distinct glycan arrays. We present data obtained from the CFG mammalian glycan array[22] and from another highly diverse glycan array containing mammalian and bacterial carbohydrate epitopes.[23] Further, the interaction was quantified in a competitive binding assay. In a next step, we demonstrated the ability of AcmJRL to bind to the SARS-CoV-2 spike protein as well as its isolated receptor-binding domain (RBD) with low-micromolar affinity in a carbohydrate-dependent manner. Further, we showed that the binding of the spike RBD to its receptor ACE2 can be inhibited by AcmJRL. Consequently, it is possible that the mannose-binding lectin AcmJRL can neutralise the SARS-CoV-2 virus through binding to its spike protein.

Results and Discussion

Isolation and characterisation of AcmJRL from bromelain

The mannophilic lectin AcmJRL was isolated by affinity chromatography from pineapple stem extract (bromelain) on a mannosylated stationary phase according to the procedure reported by Azarkan et al.[18] Prior to purification, the soluble protein fraction of bromelain was obtained by aqueous extraction in the presence of S-methyl methanethiosulfonate to block bromelain's high proteolytic activity. Using mannosylated sepharose beads[24] 0.9–1.6 mg AcmJRL were obtained per gram bromelain after elution with ᴅ-mannose.

The identity of the isolated protein was confirmed by SDS-PAGE (Figure 1A) and mass spectrometry (average molecular mass = 15346 Da, Figure 1B). The main peak (*m/z* 15388) can be assigned to an acetonitrile adduct $[M+H+MeCN]^+$ of the AcmJRL monomer. As reported by Gross et al.,[16] two additional

ChemBioChem

Research Article
doi.org/10.1002/cbic.202200463

Chemistry Europe
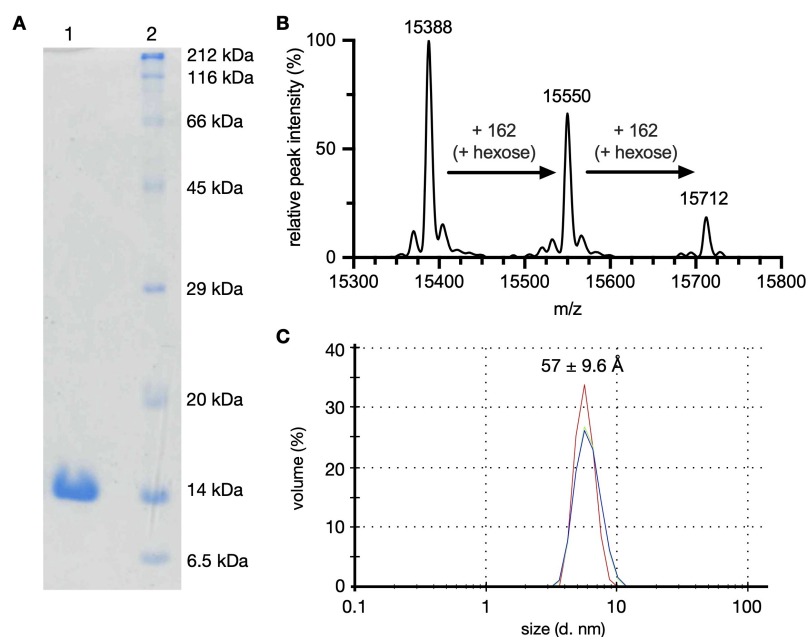European Chemical
Societies Publishing

Figure 1. A) Affinity-purified AcmJRL (lane 1) and molecular weight marker (lane 2) analysed by SDS-PAGE (18%). B) ESI-MS spectrum of AcmJRL after maximum entropy deconvolution. The main peak (m/z 15388) corresponds to an acetonitrile adduct $[M+H+MeCN]^+$. Peaks at m/z 15550 and 15712 most likely result from glycation (Figure S1). C) Dynamic-light-scattering analysis of AcmJRL (size distribution by volume). The peak at 57 ± 9.6 Å indicates dimerisation in solution, blue, green, red graphs correspond to 3 technical replicates.

mass peaks were observed in a ratio of 100:65:17, separated by a mass shift of 162 Da. During the industrial production of bromelain, the pineapple stem extract is loaded on maltodextrin, a hydrolysis product of starch, to simplify its handling. Thus, it contains carbohydrates like glucose and glucooligo-saccharides that can react with primary amines of proteins to form Schiff-bases, which is presumably followed by an irreversible Amadori rearrangement (Figure S1 in the Supporting Information) towards a stable α-amino ketone corresponding to advanced glycation end-products.[25] This glycation results in a mass increase of 162 Da that was observed in the MS-spectrum (Figure 1B). The presence of two signals of +162 and +324 Da suggests that this reaction occurred twice on the protein or one disaccharide of maltose reacted. However, it is not clear if it is a statistical mixture or if two specific lysines were affected by this reaction (5 lysines are present in AcmJRL). It was not specified whether the AcmJRL isolated and crystallised by Azarkan et al. was also glycated. Inspection of the electron density map of crystallised AcmJRL (PDB ID: 6FLY[18]) did not show evidence for unassigned electron density which could also result from a high flexibility at the protein surface or a statistical distribution of the glycation.

Previous studies showed dimerisation of AcmJRL in solution, determined by size-exclusion chromatography and equilibrium unfolding experiments.[18] However, Azarkan et al. showed that AcmJRL crystallises as a tetramer (see Introduction). We therefore used dynamic light scattering (DLS) to determine the hydrodynamic diameter of AcmJRL in buffered solution (Figure 1C). The measured hydrodynamic diameter of 57 ± 9.6 Å corresponds to the radius of the dimer (Figure S2), rather than

to monomers or tetramers. Additionally, our differential scanning fluorimetry studies suggested two unfolding events at $T_1=58$–60 °C and $T_2=73$–74 °C (Figure S2) which could reflect dissociation of the dimer followed by protein denaturation.

Glycan array analysis of AcmJRL

In general, jacalin-related lectins can be clustered by their carbohydrate specificity into galactophilic and manno-/gluco-philic subgroups. AcmJRL is reported to have a millimolar affinity towards mannosides and glucosides.[18] Glycan micro-arrays allow the simultaneous binding specificity analysis of carbohydrate-binding proteins on a library of oligosaccharides, with, for example, fluorescence labelling for optical quantification.[26]

Residues Lys50 and Lys63 are most accessible in AcmJRL for labelling with amine reactive dyes according to the solvent accessible protein surface calculated from the crystal structure (Figure S4). Fluorescence labelling with FITC resulted in a rather low labelling efficiency of 0.44. As low labelling efficiency combined with high photobleaching of fluorescein could result in poor sensitivity, we shifted to Cyanine-3 (Cy3) a pH-insensitive orange fluorescent dye. Unfortunately, Cy3-labelling via its NHS active ester also resulted in a low labelling efficiency of 0.55. Notably, one or two of the five lysines of AcmJRL are not available for labelling as they are blocked by glycation (Figure 1B). Further, the reduced accessibility of Lys6, Lys29 and Lys79 could explain the low labelling yields. On the other hand,

only about 10% of AcmJRL is bis-glycosylated, 36% is mono-glycosylated and 54% is unmodified (Figure 1B).

To elucidate its glycan specificity on a larger collection of oligosaccharides, AcmJRL was analysed on the Consortium for Functional Glycomics mammalian glycan array[22] in an updated version with 585 distinct carbohydrate epitopes (Figure 2A, Tables S5 and S6). In agreement with its known mannose specificity, the lectin showed a high affinity towards several α-mannosides (e.g., mannopentaose, CFG-GLYCAN ID **310**, Man-α-1,6(Man-α-1,3)Man-α-1,6(Man-α-1,3)Man-β, RFU = 410 ± 141).

Bi- and triantennary mannosides showed higher apparent binding affinities towards AcmJRL than monovalent glycans

(e.g., compare CFG-GLYCAN ID **312** vs. **207/209**). As described above, these oligomannosidic structures can be found in N-glycans of mammalian proteins and have been reported for viral surface proteins such as the SARS-CoV-2 spike protein. Increased binding by multivalent ligand presentation is common for glycan-lectin recognition. The mannotriose epitope Man-α-1,6(Man-α-1,3)Man (commonly present in CFG-GLYCAN ID **211**, **51** and **50**), the mannopentaose epitope Man-α-1,6(Man-α-1,3)Man-α-1,6(Man-α-1,3)Man (commonly present in in CFG-GLYCAN ID **310** and **214**) and the mannohexaose epitope Man-α-1,6(Man-α-1,3)Man-α-1,6(Man-α-1,2-Man-α-1,3)Man (present in CFG-GID **213**) showed highest binding

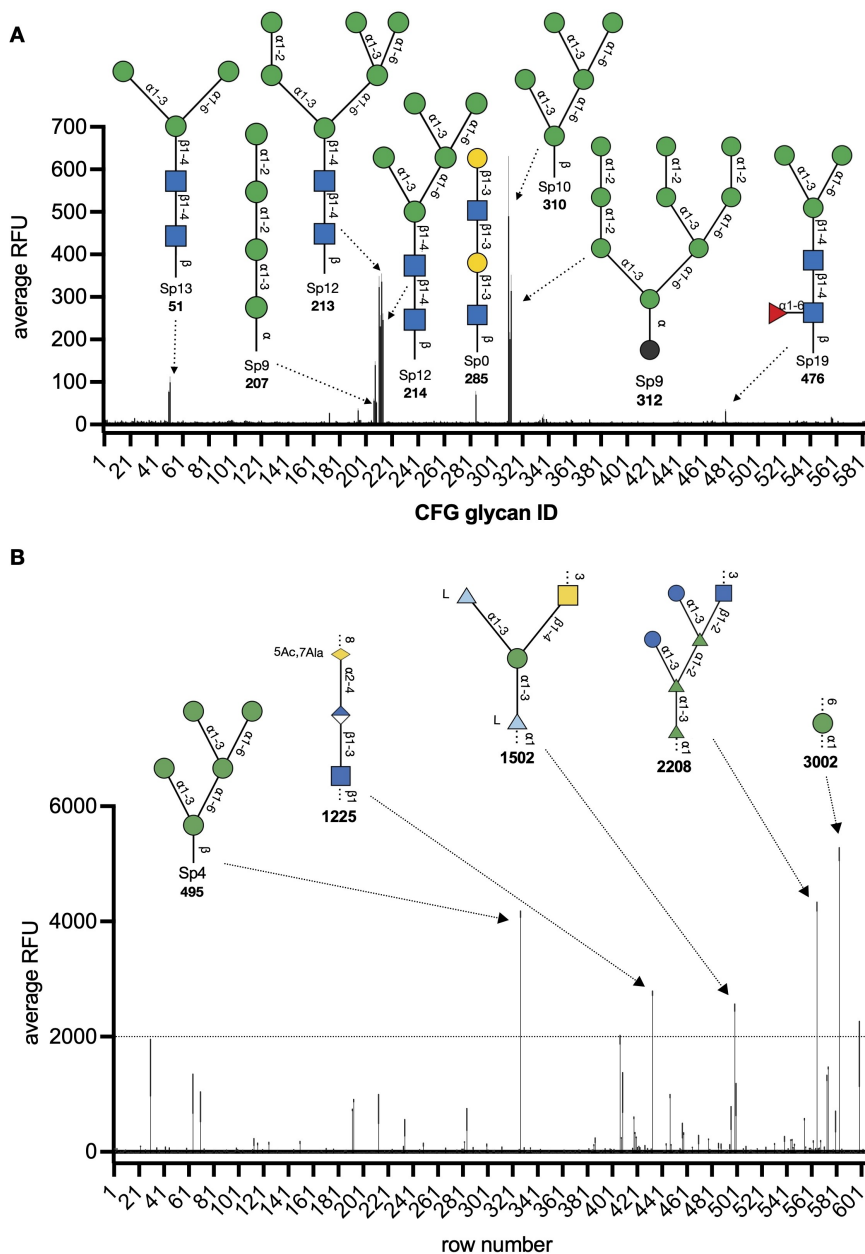**Figure 2.** Glycan array analysis of AcmJRL. A) CFG mammalian glycan array tested with FITC-labelled AcmJRL at 50 μg mL^{-1}. B) Semiotic glycan array tested with Cy3-labelled AcmJRL at 20 μg mL^{-1}. Data are presented as average RFU ± s.d. from 6 replicates on the array. RFU intensities differ between arrays because different fluorophores, protocols and scanners were used. Bold-face number = glycan ID. A translation from row number to Semiotik glycan ID and short name can be found in Tables S1 and S2.

ChemBioChem

Research Article
doi.org/10.1002/cbic.202200463

Chemistry Europe
European Chemical
Societies Publishing

responses which corresponded to reported data (K_d manno-triose = 1.4 mM, K_d mannopentaose = 590 μM).[18] One single glycan hit without mannose but a terminal β-galactoside in a LacNAc repeat (CFG-GLYCAN ID **285**, Figure 2A) is presumably a false positive due to dose-independent changes in signal intensity (5 vs 50 μg mL^{-1}).

A possible explanation for the observed specificity of AcmJRL for oligomannosides results from its dimer formation in solution and its binding of up to two mannosides per binding site. The distance between the anomeric carbons of two mannosides within one binding site is approximately 14 Å (from C1 to C1, PDB ID: 6FLY), which is similar to the distance between two mannoses in mannopentaose,[27] thus suggesting a possible chelation binding mode by this ligand. On the other hand, mannopentaose could also increase local mannose-concentration to allow the rapid rebinding to the binding sites within one monomer. The distance from the binding site of one monomer to the other monomer in the crystal structure of dimeric AcmJRL is approx. 46–50 Å and thus too far for bridging interactions within a single glycan.

Monovalent α-glucosides showed very low, but significant binding (e.g., CFG-GLYCAN ID **195**, Glc-α-1,4-Glc-β, RFU = 33 ± 5). Unfortunately, no multivalent glucosides are available on this array to understand the influence of multivalency for these epitopes.

In addition to the CFG glycan array, we analysed AcmJRL on the Semiotik glycan array,[23] which also features mammalian glycans and additionally a large variety of other glycans, mainly from bacterial species (Figure 2B). Although mannopentaose (Semiotik glycan ID (SGID) **495**) and poly-Man-α-1,6 (mannan, SGID **3002**) could be confirmed as a ligand for AcmJRL, the smaller mannotriose (SGID **258**) showed no binding, arguably due to a different length (Sp4) influencing accessibility for the protein.[28] In contrast to the CFG glycan array, a multivalent α-glucoside is present on the Semiotik chip (SGID **2208**) and was well recognised by the lectin, underlining the affinity of AcmJRL towards α-glucosides. Interestingly, two unrelated bacterial O-antigens were also recognised: *Escherichia coli* O161 (SGID **1225**, −8(D-Ala1,7)Leg5Ac-α-2,4-GlcA-β-1,3-GlcNAc-β1-) and *Aeromonas hydrophila* O34deAc (SGID **1502**, −3GalNAc-β-1,4(L-6dTal-α-1,3)Man-α-1,3 L–6dTal-α-1-). However, SGID **1502** showed a nonlinear dose-response, which requires orthogonal binding assays for verification.

Development of a competitive binding assay for AcmJRL

Glycan arrays provide valuable insight into carbohydrate specificity in high-throughput. For a quantitative binding analysis, we developed a solution-phase competitive binding assay based on our previous work for other lectins using fluorescence polarisation.[29,30,31] Fluorescein-labelled α-D-man-noside **1**[31b] was titrated with AcmJRL and a K_d of 58.9 ± 5.9 μM was determined (Figure 3). This rather high affinity of AcmJRL for this α-mannoside was surprising, compared to the lectin's reported affinity towards the previously known ligand manno-biose Man-α-1,3-Man (K_d = 2.4 mM[18]). Interestingly, such a
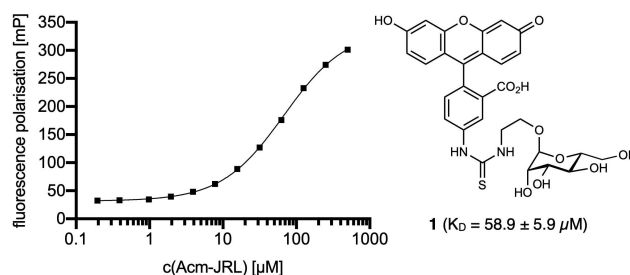
Figure 3. Direct binding of AcmJRL to mannose-based fluorescent ligand **1** and quantification by using fluorescence polarisation. The dissociation constant and standard deviations were obtained from three independent experiments in triplicates on each plate.

discrepancy between the weaker carbohydrate alone and a boost in binding affinity for its fluorophore-labelled derivative was already observed for the bacterial lectin PllA (K_d = 62.7 and 520 μM, for FITC-modified α-D-Gal and Me-α-D-Gal, respectively).[31a]

This system was used to screen several carbohydrates in competitive binding assays. Next to the carbohydrate hits D-mannose and D-glucose and the two non-recognised epitopes D-galactose and L-fucose from the glycan arrays, other plant carbohydrates like L-rhamnose (Rha), D-xylose (Xyl) and D-arabinose (Ara) were tested (Figure 4A). First, single concentration inhibition assays again confirmed the affinity of AcmJRL towards α-mannosides and α-glucosides (Figure 4A). Additionally, glucosamine (GlcN) and *N*-acetylglucosamine (GlcNAc) were confirmed as ligands. In accordance with the glycan array results, none of the other tested carbohydrates inhibited AcmJRL at 10 mM. To evaluate the influence of the glycosidic linkage of the oligomannosides (α-1,2 vs α-1,3 vs α-1,6), a titration of the appropriate dimannosides was performed. Only subtle affinity differences between the isomers could be observed (Figure 4B, IC_{50} (Man-α-1,2-Man) = 9.1 ± 0.8 mM, IC_{50} (Man-α-1,6-Man) = 11.3 ± 1.7 mM), with Man-α-1,3-Man (IC_{50} = 6.9 ± 0.6 mM) having the highest potency. Comparing the glycan array results with this finding could explain why mannopentaose which contains two Man-α-1,3-Man-epitopes was preferentially recognised over other bis-(Man-α-1,2-Man)-presenting epitopes (e.g., CFG-GLYCAN ID **208**). Interestingly, Me-α-D-glucoside (IC_{50} = 6.8 ± 0.4 mM) showed higher affinity towards AcmJRL than Me-α-D-Man (IC_{50} = 10.7 ± 0.5 mM) and the di-mannosides (Figure 4B). Furthermore, from our single point inhibition experiments it is evident that the glycosidic linkage in glucosides is crucial for recognition by AcmJRL: maltobiose (Glc-α-1,4-Glc) showed highest inhibition, whereas cellobiose (Glc-β-1,4-Glc) had no effect.

Expression of SARS-CoV-2 spike protein

Given the potential antiviral properties of plant lectins, the glycan-specificity profile of AcmJRL (see above) made us speculate about the binding of AcmJRL to the heavily glycosylated SARS-CoV-2 spike protein.
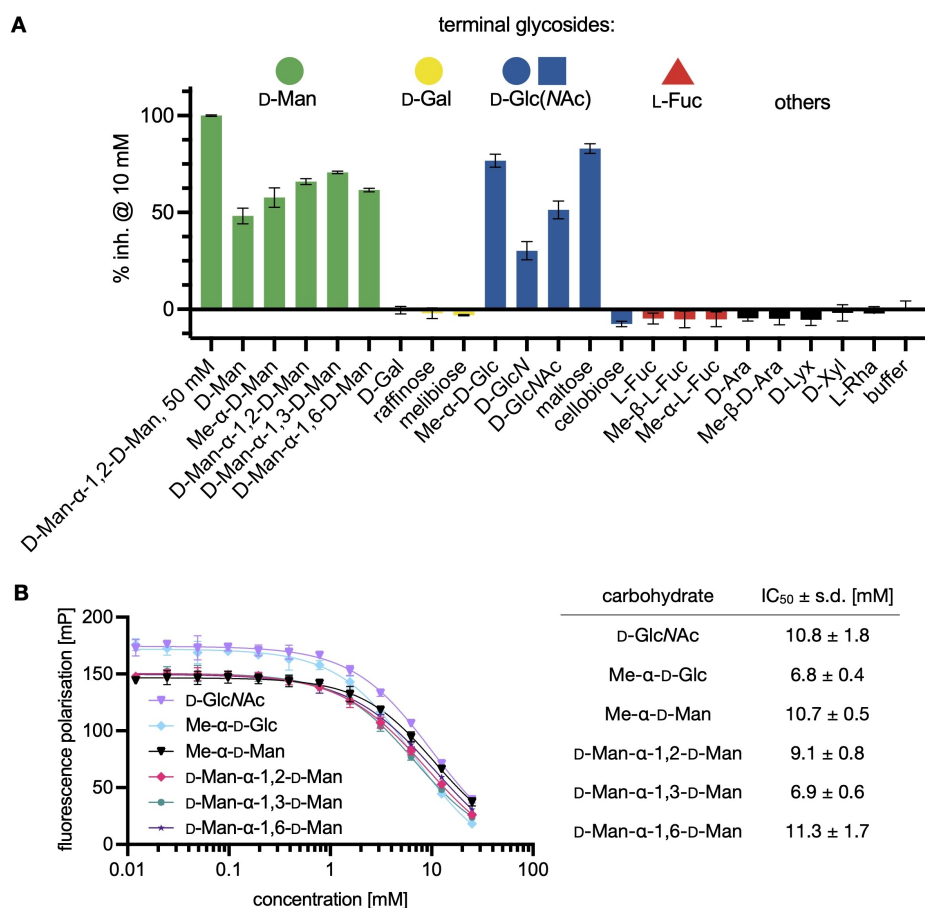
ChemBioChem

Research Article
doi.org/10.1002/cbic.202200463

**Chemistry
Europe**
European Chemical
Societies Publishing

Figure 4. Competitive binding of various carbohydrate ligands to AcmJRL. A) Inhibition of AcmJRL by a carbohydrate panel at 10 mM. Fluorescence polarisation in the presence of 50 mM Man-α1,2-Man was defined as 100% inhibition. B) Dose-response curves of AcmJRL with differently linked mannosides (left) or Me-α-Glc, GlcNAc. Data are shown as mean ± s.d. from technical triplicates on plate.

The extraviral domain of the spike-protein (S-protein) from SARS-CoV-2 was recombinantly produced in HEK293[32] cells using a pCAGGS-based eukaryotic vector system yielding 1.42 mg glycoprotein from one batch of 560 mL. HEK293 cells were used as expression system due to the established protocol by Walls et al.[32] and its detailed glycosylation analysis by Watanabe et al..[7]

Identity and purity of the protein were determined by gel electrophoresis (Figure 5A) and mass spectroscopy (Figure 5B). Both experiments coherently showed a molecular weight around 145 kDa. Interestingly, mass spectroscopy revealed four major masses after maximum entropy (MaxEnt) deconvolution of the centroided mass spectrum, each separated by approximately 2 kDa (Figure 5B). As described above, S-protein usually exhibits highly complex glycosylation, which leads to a non-homogeneous sample. Therefore, the heterogeneous mass distribution determined by ESI-MS presumably resulted from the presence of different glycoforms.

Peptide-N-glycanase F (PNGase F) specifically hydrolyses amide bonds between the reducing end of GlcNAc and asparagine residues of N-glycans. Thus, PNGase F was used to prove the presence of N-glycans on the recombinantly produced S-protein (Figure 5). The treatment resulted in a faster migration of the S-protein on the SDS gel indicating a molecular weight reduced by several kDa (Figure 5A). The MaxEnt deconvoluted mass spectrum of the treated S-protein also showed a mass shift of approximately 7 kDa, resulting in a major peak around 138 kDa. Notably, all mass peaks of the PNGase F-treated species were much sharper and reached higher signal intensities compared to the native protein, indicating a reduction of microheterogeneity of the glycoforms.

Mannose-dependence of AcmJRL binding to SARS-CoV-2 spike-protein

After verification of the S-protein identity, a biophysical assay for determination of binding kinetics and affinity of AcmJRL to the S-protein was established. Given the high molecular weights of both interaction partners, surface plasmon resonance (SPR) analysis was chosen to determine binding affinity and kinetics of AcmJRL against immobilised S-protein.

Single cycle kinetics were performed by injecting AcmJRL at increasing concentrations from 2.5 to 20 μM onto a sensor chip with immobilised S-protein and a dose-dependent response was observed. Even at the highest concentration, saturation
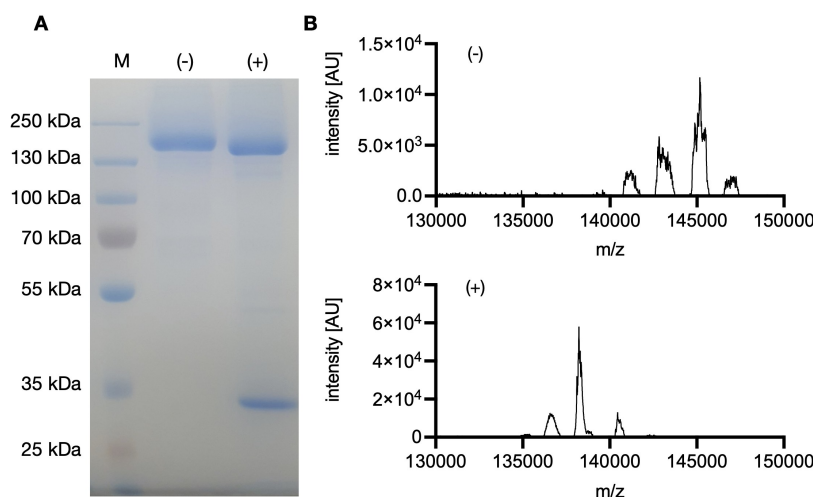
ChemBioChem

Research Article
doi.org/10.1002/cbic.202200463

Chemistry
Europe
European Chemical
Societies Publishing

Figure 5. A) SDS-PAGE (10%) of native S-protein (−) and S-protein digested with PNGase F (+). B) Deconvoluted mass spectrum of native S-protein (−) and S-protein digested with PNGase F (+). In both experiments, a mass shift of several kDa is visible after treatment with PNGase F, thus indicating the removal of N-glycans.

could not be observed after 120 seconds of association, hinting at an extensive number of available binding sites for AcmJRL. In addition, only an incomplete dissociation was recorded during the dissociation phases. The association rate (k_{on}) was 1057 ± 93 $M^{-1}s^{-1}$, the dissociation rate (k_{off}) was $3.4 \pm 0.4 \times 10^{-3}$ s^{-1} which corresponds to a K_D of 3.3 ± 0.6 μM. A similar K_D of 11.1 ± 2.5 μM was determined after fitting the response after 115 seconds of contact time of the association with the Langmuir isotherm.

Interestingly, the K_D increased gradually for each single experiment performed for the technical replicates (dissociation constants calculated from Langmuir isotherm: 7.9, 11.5, 14.0 μM; apparent dissociation constants calculated from rate constants: 2.7, 3.1, 4.0 μM). This observation likely resulted from some AcmJRL remaining bound during the regeneration cycles

as the S-protein has a vast number of possible binding sites in its numerous N-glycans for AcmJRL. Furthermore, during dissociation phases the response did not fully decrease to the baseline level, indicating an incomplete dissociation of AcmJRL.

As AcmJRL interacts with the mannotriose epitope (Man-α-1,6(Man-α-1,3)Man, present in CFG glycan ID **211**, **213**, **51** and **50**) in the glycan array analysis, single cycle kinetics of AcmJRL with the addition of 10 mM mannotriose in the sample buffer were also conducted to analyse the glycan-dependence of the AcmJRL-spike binding. The loss of observable binding to the spike protein in the presence of the competitor demonstrates the mannose-dependent binding of AcmJRL to the spike protein (Figure 6). In fact, even 1 and 5 mM mannotriose significantly reduced the interaction of AcmJRL with S-protein in a dose-dependent manner (Figure S6). An unspecific inhib-
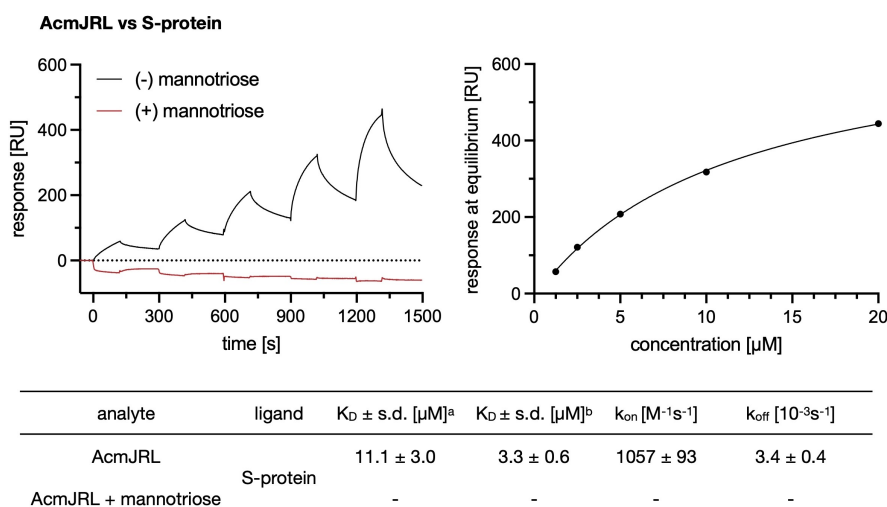

analyte	ligand	$K_D \pm$ s.d. [μM][a]	$K_D \pm$ s.d. [μM][b]	k_{on} [$M^{-1}s^{-1}$]	k_{off} [$10^{-3}s^{-1}$]
AcmJRL	S-protein	11.1 ± 3.0	3.3 ± 0.6	1057 ± 93	3.4 ± 0.4
AcmJRL + mannotriose		-	-	-	-

Figure 6. SPR sensorgrams of the binding of AcmJRL to immobilised S-protein in the absence (black) and presence of 10 mM mannotriose (=Man-α-1,6(Man-α-1,3)Man, red) and Langmuir graph of AcmJRL binding to S-protein. [a] Dissociation constant calculated from Langmuir isotherm or [b] apparent dissociation constant calculated from rate constants, $K_D = k_{off}/k_{on}$.

ChemBioChem

Research Article
doi.org/10.1002/cbic.202200463

Chemistry Europe
European Chemical
Societies Publishing

ition of the AcmJRL–S-protein interaction by high carbohydrate-concentrations was excluded by the use of the disaccharide D-lactose (Gal-β-1,4Glc) and the trisaccharide D-raffinose (Gal-α-1,6Glc-α-1,2Fruc) as negative controls, which did not interfere with the AcmJRL-spike interaction (Figure S6)

AcmJRL binds to SARS-CoV-2 spike RBD and to its native receptor ACE2

The RBD of the S-protein is essential for the SARS-CoV-2 infection process, as it mediates binding to the human cell-surface receptor ACE2, allowing the attachment of the virus. As we observed the binding of AcmJRL to the S-protein, we set out to determine if the lectin is able to block this essential mechanism for the infection through binding to the spike protein. Complex glycosylation is present in many other human cell-surface proteins, such as the receptor ACE2.

Consequently, we also analysed the binding of AcmJRL to ACE2 as well as to spike RBD produced for interaction studies. Single cycle kinetics on SPR were performed for AcmJRL binding to both the S-protein RBD and the human ACE2 receptor (Figure 7). Twenty one N-glycosylation sites are present in full length S-protein (per monomer, 63 in the trimeric form) literally leading to a sweet fur covering the entire spike,[5,6] two of which reside within its RBD.[9] The observed association

of AcmJRL to S-protein RBD reflects this reduced glycosylation well, as saturation was now reached during association. The determined K_D value of 12.9 μM from kinetics or 35 μM from the Langmuir plot is about threefold higher compared to its interaction with full length extraviral domain of the S-protein. The association kinetics ($k_{on} = 1490 \pm 455$ M^{-1}s^{-1}) were comparable to those for AcmJRL binding to S-protein (Figure 6). However, the dissociation of AcmJRL from spike RBD is about fourfold faster, displayed in the determined $k_{off} = 19.4 \pm 6.7 \times 10^{-3}$ s^{-1}, a consequence of the reduced extent of glycosylation of the RBD.

Human ACE2 is also highly glycosylated, carrying more matured complex glycans compared to the high-mannose enriched virus surface protein.[33] From SPR analysis of AcmJRL binding to immobilised recombinant ACE2 produced in HEK293 cells, we obtained a K_D value of 22.1 ± 5.3 μM calculated from the Langmuir isotherm, which is sevenfold higher than the one obtained for binding to the S-protein. This observation could be a direct result of the altered glycosylation pattern of this human receptor that is distinct from the viral proteins. The association rate of AcmJRL to ACE2 ($k_{on} = 590 \pm 212$ M^{-1}s^{-1}) was also slower compared to the one for the S-protein. Further, the threefold higher dissociation rate ($k_{off} = 12.2 \pm 1.0 \times 10^{-3}$ s^{-1}) of AcmJRL from the ACE2 receptor indicates a faster dissociation of the complex. In contrast to the interaction with full length S-protein, complete dissociation of AcmJRL from both the RBD
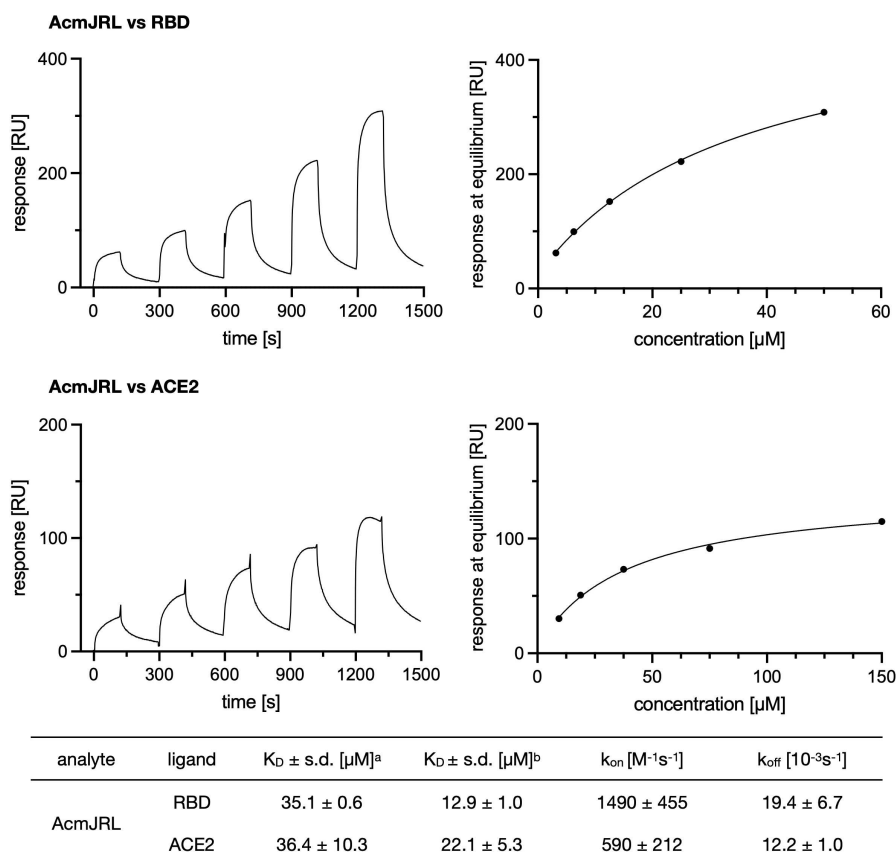

analyte	ligand	$K_D \pm$ s.d. [μM][a]	$K_D \pm$ s.d. [μM][b]	k_{on} [M^{-1}s^{-1}]	k_{off} [10^{-3}s^{-1}]
AcmJRL	RBD	35.1 ± 0.6	12.9 ± 1.0	1490 ± 455	19.4 ± 6.7
	ACE2	36.4 ± 10.3	22.1 ± 5.3	590 ± 212	12.2 ± 1.0

Figure 7. SPR sensorgrams with Langmuir graphs of the binding of AcmJRL to S-protein RBD (top) and ACE2 receptor (bottom). [a] Dissociation constant calculated from Langmuir isotherm or [b] apparent dissociation constant calculated from the rate constants, $K_D = k_{off}/k_{on}$.

ChemBioChem

Research Article
doi.org/10.1002/cbic.202200463

**Chemistry
Europe**
European Chemical
Societies Publishing

and ACE2 complexes was observed. The observed affinity of AcmJRL for both S-protein and ACE2 could therefore result in a synergistic inhibitory effect on viral cell entry.

AcmJRL weakens the interaction of spike RBD with ACE2

The interaction between the spike RBD and its ACE2 receptor is characterised by nanomolar affinity and is essential for the infection process. As AcmJRL binds the S-protein RBD and ACE2 with low-micromolar affinity, it is likely that the spike interaction with ACE2 could be inhibited by AcmJRL. To test this hypothesis, we first reproduced the affinity reported for the S-protein RBD to the immobilised ACE2 receptor (Figure 8) by SPR and obtained a K_D of 10.9 nM.[34]

The influence of AcmJRL on the affinity of S-protein RBD binding to the ACE2 receptor was studied by an addition of AcmJRL with a molar excess of lectin (factor 10 and 100, i.e., 1 and 10 μM Figure 8) to the RBD and preincubation prior to injection. Then, a single cycle kinetics run with injections of five dilutions (6.25 nM RBD with 10- and 100-fold excess AcmJRL – 100 nM RBD with 10- and 100-fold excess AcmJRL) of the RBD-AcmJRL mixture was performed with immobilised ACE2 receptor. Although residual binding of RBD to ACE2 receptor could still be observed (Figure 8), its apparent affinity was reduced by a factor of two ($K_D = 21.1 \pm 2.9$ nM) after preincubation with a tenfold excess of AcmJRL. An increase to a 100-fold excess of preincubated AcmJRL led to another twofold decrease in K_D value to 37.1 ± 4.7 nM. This rather moderate inhibitory effect probably resulted from the dilution of the preincubation mixture into the different injected concentrations, resulting in AcmJRL concentrations below the determined K_D values of AcmJRL for spike RBD and ACE2. The addition of sufficiently high concentrations of AcmJRL to saturate RBD could not be used to overcome this problem, since AcmJRL also directly binds to the glycans of the immobilised ACE2 impacting on the recorded SPR response.

In a clinical scenario, saturating both the glycans of ACE2 and spike with AcmJRL could be beneficial to weaken the virus-host interaction and provide the immune system with an added advantage while battling the infection, e.g. by nasal or pulmonal application.

Conclusions

The current SARS-CoV-2 pandemic is a serious crisis that urgently asks for therapeutic treatment options. The viral envelope of SARS-CoV-2 is densely covered by the highly glycosylated spike protein, which is essential for viral cell entry through binding to the ACE2 receptor.

In this work, the pineapple-derived jacalin-related lectin AcmJRL was purified from the active pharmaceutical ingredient bromelain and characterised by mass spectrometry, differential scanning fluorimetry and dynamic light scattering. We further analysed the lectin's ligand specificity by glycan-array analysis using two complementary arrays. The data further supported the previously reported preference of AcmJRL for mannopen-taose. A solution-phase binding assay was subsequently developed to quantify AcmJRL-carbohydrate interactions.

Then, the interaction of AcmJRL with recombinantly produced SARS-CoV-2 spike protein was studied by surface plasmon resonance analysis. The low-micromolar binding was carbohydrate-dependent and could be inhibited by supplementation with mannotriose. Finally, we could show that addition of AcmJRL reduced the tight binding affinity of the spike RBD for

RBD vs ACE2

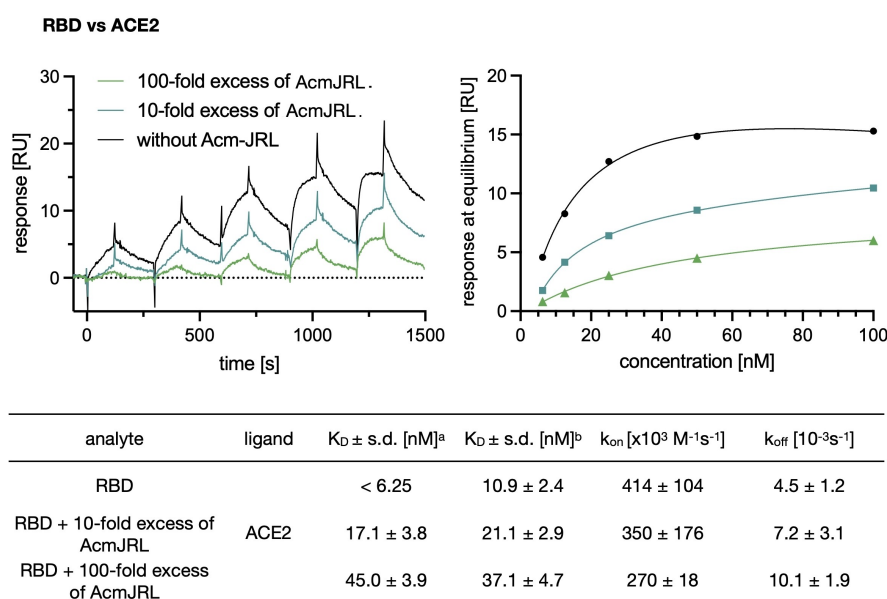| analyte	ligand	$K_D \pm$ s.d. [nM][a]	$K_D \pm$ s.d. [nM][b]	k_{on} [×10³ M⁻¹s⁻¹]	k_{off} [10⁻³s⁻¹]
RBD		< 6.25	10.9 ± 2.4	414 ± 104	4.5 ± 1.2
RBD + 10-fold excess of AcmJRL	ACE2	17.1 ± 3.8	21.1 ± 2.9	350 ± 176	7.2 ± 3.1
RBD + 100-fold excess of AcmJRL		45.0 ± 3.9	37.1 ± 4.7	270 ± 18	10.1 ± 1.9

Figure 8. SPR sensorgrams and corresponding affinity plots for the binding of S-protein RBD to immobilised ACE2 (black). Prior to injection, S-RBD was also preincubated with a 10-fold (blue) or 100-fold (green) excess of AcmJRL. [a] Dissociation constant calculated from Langmuir isotherm or [b] apparent dissociation constant calculated from rate constants, $K_D = k_{off}/k_{on}$.

ChemBioChem

Research Article
doi.org/10.1002/cbic.202200463

Chemistry Europe
European Chemical
Societies Publishing

the human ACE2 receptor. Thus, bromelain and specifically its component AcmJRL could constitute a novel antiviral drug or adjuvant in combination therapy to neutralise SARS-CoV-2 post exposure.

Experimental Section

Bromelain was supplied by Ursapharm (Saarbrücken, Germany). Mannotriose ($>95\%$), Me-α-L-Fuc ($>98\%$), Me-β-L-Fuc ($>98\%$) were obtained from Carbosynth Ltd. (UK); D-glucosamine, D-mannose, D-galactose, D-Man-α-1,2-D-Man, D-Man-α-1,3-D-Man and D-Man-α-1,6-D-Man were obtained from Dextra Laboratories Ltd. (UK); Me-α-D-Glc ($\geq99\%$) and D-xylose ($\geq99\%$) was obtained from Sigma-Aldrich; Me-β-D-Ara ($>99\%$) and maltose ($>98\%$) were obtained from TCI Europe (Belgium); cellobiose ($\geq98\%$) was obtained from Carl Roth; L-rhamnose ($>99\%$) was obtained from AppliChem GmbH (Germany); melibiose was obtained from Alfa Aesar; D-lyxose was obtained from Acros Organics (Belgium) and N-acetyl D-glucosamine was obtained from MP Biomedicals (France); raffinose ($>99\%$) was obtained from Th. Geyer GmbH & Co. KG (Germany); D-arabinose ($>98\%$) was obtained from Abcam (UK); L-fucose was obtained from Jennewein Biotechnologie GmbH (Germany).

Preparation of D-mannosylated sepharose: D-Mannosylated sepharose was synthesised according to the protocol of Fornstedt and Porath:[24] Sepharose CL-6B beads (Sigma-Aldrich, 15 mL) were suspended in Na_2CO_3-buffer (500 mM, pH 11, 15 mL). Divinylsulfone (1.5 mL) was added, and the suspension was stirred at RT for 70 min. Activated sepharose was extensively washed with water and resuspended in 15 mL aqueous D-Mannose solution (20% m/v, 500 mM Na_2CO_3, pH 10). The reaction was stirred over night at RT, filtered and extensively washed with water. Unreacted activated sepharose was quenched by addition of β-mercaptoethanol (300 µL) in buffer (15 mL, 500 mM $NaHCO_3$, pH 8.5) for 120 min. After filtration and washing of the mannosylated beads, they were filled into 5 mL plastic columns for affinity chromatography.

Isolation of AcmJRL from bromelain: AcmJRL was isolated in analogy to the protocol of Azarkan et al.[18] Bromelain powder (28 g) was suspended in an Erlenmeyer flask in buffer (400 mL, 100 mM NaOAc pH 5, 1 mM EDTA, 20 mM methyl methanethiosulfonate) and stirred for 60 min at RT. After centrifugation (30000 rcf, 30 min, 4 °C), the supernatant was dialysed twice for 1 h against 4 L Tris-buffered saline (TBS: 150 mM NaCl, 50 mM Tris pH 7.4). The sample was loaded on a D-mannosyl-sepharose column pre-equilibrated with the dialysis buffer. After extensive washing, the lectin was eluted with 1 M D-mannose in buffer. Eluted fractions containing AcmJRL were pooled and dialysed against TBS (5×3 h against 2 L). The yield (31 mg) was determined by UV-absorption at 280 nm (MW = 15.34 kDa, $\varepsilon = 19940$ $M^{-1}\times cm^{-1}$).

Intact protein mass determination: Intact protein mass measurements for AcmJRL were performed on a Dionex Ultimate 3000 RSLC system using an Aeris Widepore XB C8, 150×2.1 mm, 3.6 µm dp column (Phenomenex, USA). Separation of a 2 µL sample was achieved by a linear gradient from A) $H_2O + 0.1\%$ formic acid to B) MeCN $+ 0.1\%$ formic acid at a flow rate of 300 µL min^{-1} and 45 °C. The gradient was initiated by a 1 min isocratic step at 2% B, followed by a linear increase to 75% B in 10 min to end up with a 3 min step at 75% B before re-equilibration with initial conditions. UV spectra were recorded by a DAD in the range from 200 to 600 nm. The LC flow was split to 37.5 µL min^{-1} before entering the maXis 4G hr - ToF mass spectrometer (Bruker Daltonics, Bremen, Germany) using the standard Bruker ESI source. In the source region, the temperature was set to 200 °C, the capillary voltage was

4000 V, the dry-gas flow was 5.0 L min^{-1} and the nebuliser was set to 1.0 bar. Mass spectra were acquired in positive ionisation mode ranging from 150–2500 m/z at 2.0 Hz scan rate. Protein masses were deconvoluted by using the Maximum Entropy algorithm (Spectrum Square Associates, Inc.).

Dynamic light scattering: Dynamic light scattering (DLS) measurements were performed on a Zetasizer Nano-ZS (MalvernInstruments, UK). Protein solutions were filtered with a syringe filter (0.45 µm) before measurements. AcmJRL (14 µM) was measured in TBS (150 mM NaCl, 50 mM Tris pH 7.4) at 25 °C.

Differential scanning fluorimetry: 20 µL of a solution containing AcmJRL (20 µM) and SyproOrange (final concentration 10x of a 5000x stock in DMSO, Sigma-Aldrich) in TBS (150 mM NaCl, 50 mM Tris pH 7.4) was added to a white semi-skirted 96-well plate (ThermoFisher) in triplicate. The melting curve measurements (25–95 °C, 0.5 °C min^{-1}) were performed and analysed on a real time PCR instrument (StepOnePlus, Applied Biosystems).

Direct binding of fluorescent mannoside ligand 1 to AcmJRL: Fluorescent ligand 1[31b] was dissolved in DMSO, then diluted to a final concentration of 200 nM in TBS (150 mM NaCl, 50 mM Tris pH 7.4). AcmJRL was concentrated (Vivaspin column, 10000 MWCO, Sartorius Stedim Biotech GmbH, Germany) to a concentration of 1.33 mM in TBS. After centrifugation (10 min, 25000 rcf, RT), the concentration of AcmJRL was adjusted to 1 mM as determined by UV absorbance measurement at 280 nm ($\varepsilon = 19,940$ M^{-1} cm^{-1}). A serial dilution of AcmJRL was dispensed in triplicate (10 µL each) in a black 384-well plate (Greiner Bio-One, Germany, cat no 781900). The solution of the fluorescent ligand (10 µL) was added to yield a final concentration of 100 nM. After incubation for 1 h at RT, fluorescence ($\lambda_{ex} = 485$ nm, $\lambda_{em} = 535$ nm) was measured in parallel and perpendicular to the excitation plane on a PheraStar FS plate reader (BMG Labtech GmbH, Germany) and polarisation was calculated. The data were analysed by using a four-parameter fit calculated with MARS Data Analysis Software (BMG Labtech). Three independent experiments were performed on three plates.

Reporter ligand displacement assay: The assay for AcmJRL was performed in analogy to the protocol for LecA from Joachim et al.[29] A serial dilution of the test compounds was prepared in TBS (150 mM NaCl, 50 mM Tris pH 7.4). For single point inhibition measurements, carbohydrates were dissolved in TBS at 20 mM. A concentrated solution of AcmJRL was diluted in TBS together with the fluorescent reporter ligand 1 to yield concentrations of 40 µM protein and 20 or 200 nM ligand, respectively. 10 µL of this mix was added to 10 µL previously prepared dilutions of the test compounds in black 384-well microtiter plates (Greiner Bio-One, Germany, cat. no. 781900) in triplicate. After centrifugation (2680 rcf, 1 min, RT), the reactions were incubated for 60 min at RT in a humidity chamber. Fluorescence ($\lambda_{ex} = 485$ nm, $\lambda_{em} = 535$ nm) was measured in parallel and perpendicular to the excitation plane on a PheraStar FS plate reader (BMG Labtech). The measured intensities were reduced by the values of only AcmJRL in TBS, and fluorescence polarisation was calculated. The data were analysed with the MARS Data Analysis Software and fitted according to the four-parameter variable slope model. Bottom and top plateaus were fixed according to the highest concentration of mannoside, and the data was reanalysed with these values fixed.

Fluorescence labelling of AcmJRL

FITC: AcmJRL was diluted in Na_2CO_3 buffer (100 mM, pH 9.3) and concentrated (Vivaspin, Sartorius Stedim Biotech GmbH, 10000 MWCO) to yield a final protein concentration of 78 µM

ChemBioChem

Research Article
doi.org/10.1002/cbic.202200463

Chemistry Europe
European Chemical
Societies Publishing

(1.8 mg in 1.5 mL). FITC (Merck, Germany, 95 μL of a freshly prepared 7.7 mM solution in carbonate buffer pH 9.3, 0.73 μmol, 6.2 equiv.) was added and incubated for 1 h at RT. The reaction was quenched with ethanolamine (1 μmol, 8.3 equiv.) for 1 h at RT. Excess reagents were removed by filtration (Vivaspin, 10 000 MWCO). Then, the protein was affinity-purified as described above for unlabelled AcmJRL. The protein concentration and degree of labelling (DOL) were calculated from equations (1) and (2) according to the manufacturers protocol (Thermo Scientific, Rockford, USA):

$$c = \frac{A_{280\ nm} - A_{495\ nm}*k}{\varepsilon^{280\ nm}} \qquad (1)$$

$$DOL = \frac{A_{495\ nm}}{\varepsilon_{FITC}^{495\ nm}*c} \qquad (2)$$

$A_{280\,nm}$ Absorption of labelled protein at 280 nm
$A_{495\,nm}$ Absorption of labelled protein at 495 nm
$\varepsilon^{280\,nm}$ extinction coefficient of unlabelled protein at 280 nm
$k = 0.3$ correction factor for FITC
$\varepsilon_{FITC}^{495\ nm} = 68000\,\frac{L}{mol*cm}$ extinction coefficient of FITC at 495 nm

NHS-activated Cy3: AcmJRL was diluted in PBS pH 8.4 and concentrated (Vivaspin, Sartorius Stedim Biotech GmbH, 10,000 MWCO) to yield a final protein concentration of 293 μM (4.5 mg in 1.5 mL). NHS-activated Cy3 (Lumiprobe, Germany, 75 μL of a freshly prepared 29 mM solution in DMSO, 2.2 μmol, 9 eq.) was added and incubated for 5 h at RT. Excess reagents were removed by filtration (Vivaspin, Sartorius Stedim Biotech GmbH, 10 000 MWCO), then the protein was affinity-purified as described above for unlabelled AcmJRL. The protein concentration and degree of labelling (DOL) was calculated as described above.

$k = 0.08$ correction factor for Cy3

$\varepsilon_{Cy3}^{550\ nm} = 150000\,\frac{L}{mol*cm}$ extinction coefficient of Cy3 at 550 nm

Glycan array analysis: FITC-labelled AcmJRL was tested by the National Center for Functional Glycomics (NCFG, Boston, MA, USA) on the CFG glycan microarray version 5.5 containing 585 printed glycans in replicates of 6. Standard procedures of NCFG (details see https://ncfg.hms.harvard.edu/files/ncfg/files/protocol-direct_glycan_binding_assay-cfg_slides.docx) were run with 5 and 50 μg mL^{-1} protein based on the protocol by Blixt et al.[22] Raw data (Tables S5 and S6) will be shared online on the CFG website (CFG #3693).

Cy3-labelled AcmJRL was tested in-house on a glycan microarray slide from Semiotik LLC (Moscow, Russia) containing 610 printed glycans in replicates of 6. Standard procedures were run at 20, 200 and 400 μg mL^{-1} based on the protocol by Olivera-Ardid et al..[23] Fluorescence intensity was measured at 565 nm upon excitation at 520 nm on a Sapphire Biomolecular imager (Azure Biosystems, Dublin, CA, USA) at 10 μm resolution. Scan data were processed with ScanArray software (PerkinElmer) by using OSPS090418_full.360.80um.gal (kindly provided by

Semiotik) for dot-glycan assignment. Raw data (dot mean fluorescence intensity) was processed by GraphPad Prism 9 (GraphPad Software). Processed data in table format are provided in the appendix.

Protease activity assay: Purified AcmJRL was used and adjusted to $A_{280\ nm} = 1$. For the positive control, 2 mg bromelain powder were suspended in 2 mL buffer (100 mM KCl, 5 mM KOAc, 5 mM HOAc, pH 4.6) and incubated at 37 °C, 500 rpm on a Thermomixer (Eppendorf, Germany) for 10 min. After centrifugation (17 600 rcf, 10 min, RT) the supernatant was adjusted to $A_{280\ nm} = 1$. Then, 4 μL protein or bromelain extract was diluted in 200 μL buffer. Z-Lys-ONP (Merck, 4 μL from a 25 mM solution in H$_2$O/MeCN 1:1) was added and absorption at 340 nm was measured on a CLARIOstar microplate reader (BMG Labtech) for 300 s (5 s interval). Blank controls without added protein/bromelain and substrate were performed for background subtraction. Data was analysed by using GraphPad Prism 9 (GraphPad Software).

Cloning and recombinant expression of SARS-CoV-2 spike protein: A synthetic DNA fragment was purchased from Eurofins MWG. The nucleotide sequence was codon optimised for mammalian cell expression (translational amino acid sequence based on PDB ID: 6VXX[32]). The nucleotide sequence coding for the extraviral domain of SARS-CoV-2 spike (coding for aa 1–1213) was amplified via PCR with the restriction sites 5′-BamHI/XhoI-3′ (Fw Primer: ATAT<u>GGATCC</u>ATGTTCGTGTTCCTGGTTCTT; Rv Primer: AATATGAGCAGTACATAAAATGGCCC<u>CTCGAG</u>ATAT; purchased from Merck). As vector system, the in-house vector πα-SHP–H (provided by Dr. Jesko Köhnke, pCAGGS based, NCBI accession number: LT727518) was chosen for the mammalian expression system. The amplicon was digested with the respective restriction enzymes (ThermoFisher) and ligated with T4 Ligase (ThermoFisher) into the linearised πα-SHP–H vector to clone πα-SHP–H-Sgene with an N-terminal octahistidine tag.

The mammalian cell line HEK 293/T served as host for recombinant production of the glycoprotein. The cells were cultured with Dulbecco's modified Eagle medium (DMEM, Sigma Aldrich) in a Hyperflask M ($A = 1720\ cm^2$, Corning) and incubated at 37 °C under 5 % CO$_2$ atmosphere until a confluence of 80–90 % was reached. The transient mammalian transfection was applied in a mass ratio of 1:2 πα-SHP–H-Sgene/PEI (linear, MW > 25 000, Alfa Aesar).[35] After 5 h incubation, the medium was exchanged and the transfected cell line was incubated for 48 h at 37 °C under 5 % CO$_2$ before the supernatant was filtrated (0.22 μm pore size) and stored on ice. The supernatant was loaded onto a 5 mL HisTrap HP column and washed with 20 column volumes lysis buffer (200 mM NaCl, 20 mM Tris, 20 mM imidazole pH 8) and the protein was obtained with elution buffer (200 mM NaCl, 20 mM Tris, 500 mM imidazole pH 8). Size-exclusion chromatography was performed on a HiLoad 16/600 Superdex 200 PG. The elution volume of 60–70 mL was collected and the solution was concentrated to a volume of 200 μL with an Amicon Ultra-15 PLHK Ultracel-PL Membrane 100 kDa (Merck) spin column. The amount of SARS-CoV-2 spike protein was determined via UV absorbance measurement on a Nanodrop 2000c to a mass concentration of 7.1 mg/mL ($\varepsilon = 141.35 \times 10^3\ M^{-1} \cdot cm^{-1}$; MW = 142.13 kDa). For SDS-PAGE, 20 μL

ChemBioChem

Research Article
doi.org/10.1002/cbic.202200463

Chemistry Europe
European Chemical
Societies Publishing

(6 µg) of SARS-CoV-2 spike protein (in 150 mM NaCl, 20 mM HEPES pH 8) was mixed with 4 µL 6x SDS-loading buffer (1.2 g SDS, 6 mg bromophenol blue, 4 mL glycerol, 0.6 mL 1 M Tris pH 8.0, 5.4 mL H_2O, 930 mg dithiothreitol) and heated for 2 min at 100 °C, afterwards cooled to RT. A SDS-PAGE gel (10 % v/v polyacrylamide) was loaded with 20 µL of the prepared sample. 6 µL PageRulerPlus Prestained Protein Ladder (ThermoFisher Scientific) was loaded to monitor the progress of the SDS-PAGE and to estimate the approximate size of the protein after staining the gel. The SDS-PAGE was run in a Mini-PROTEAN Tetra System (BIO RAD) with SDS buffer at 150 V for 100 min. The gel was stained with Coomassie.

Deglycosylation with PNGase F: To 5 µg of spike-protein in 20 µL of 50 mM sodium phosphate buffer (pH 7.5), 2 µL (1000 U) PNGase F (New England Biolabs) were added and the reaction was incubated for 6 h at 37 °C. As a negative control, the same amount of spike-protein was incubated in absence of enzyme in otherwise identical conditions.

Surface plasmon resonance: SPR experiments were conducted on a Biacore X100-system (GE Healthcare). SARS-CoV-2 spike-protein was immobilised on a CM5 sensor chip after EDC/NHS activation by amine coupling (0.5 M 1-ethyl-3-(3-dimethylamino-propyl) carbodiimide hydrochloride and 0.1 M N-hydroxysuccinimide in water for activation). The glycoprotein was dissolved in 10 mM sodium acetate pH 4.5 (50 µg mL^{-1}) and injected over the activated chip surface (contact time of 200 s, flow rate of 30 µL min^{-1}), followed by ethanolamine for deactivation of excess reactive NHS ester groups to obtain a final response of ~6700 RU (2626 RU for Figure S6). The ACE2 receptor (Sigma-Aldrich, SAE0064) was immobilised on a CM5 sensor chip using the same conditions and a final response of ~990 RU was obtained. The SARS-CoV-2 spike RBD (Thermo-Fisher) was immobilised on a CM5 sensor chip under the same conditions and a final response of ~1970 RU was obtained. SPR assays were performed with a flow rate of 30 µL min^{-1} in HBS-EP (150 mM NaCl, 10 mM HEPES pH 7.4, 3 mM EDTA, 0.005 % Polysorbate-20). Increasing concentrations of AcmJRL (1.25, 2.5, 5.0, 10.0, 20 µM)-alone or in the presence of 10, 5 or 1 mM mannotriose, or 10 mM raffinose or 10 mM lactose-were injected for single cycle measurements (120 s contact time, 180 s dissociation time). Respectively, increasing concentrations of RBD (6.75–100 nM) with or without AcmJRL in a molar ratio of RBD/AcmJRL of 1:10 and 1:100 were injected for single cycle measurements (120 s contact time, 180 s dissociation time). The CM5 chip surface was regenerated by one injection of ethylene glycol 80 % v/v (contact time 30 s, flow rate 30 µL min^{-1}, followed by 2 injections of HBS-EP (60 s, flow rate 30 µL min^{-1}). Binding analysis results were evaluated using the Biacore X100 evaluation software to plot the sensorgrams and the Langmuir graphs, and to determine apparent dissociation constants. Graphs were visualised with GraphPad Prism 9 software (Graph-Pad Software, San Diego, CA, USA). Spikes caused by instrumental effects were removed by omitting 3–5 s around each injection.

Conflict of Interest

Peter Meiser is an employee of Ursapharm, which has funded parts of this research.

Data Availability Statement

The data that support the findings of this study are available in the supplementary material of this article.

[1] M. A. Kim, Y. W. Lee, S. R. Kim, J. H. Kim, T. K. Min, H. S. Park, M. Shin, Y. M. Ye, S. Lee, J. Lee, J. H. Choi, G. C. Jang, Y. S. Chang, *Allergy, Asthma Immunol. Res.* 2021, *13*, 526–544.

[2] L. Wang, N. A. Berger, P. B. Davis, D. C. Kaelber, N. D. Volkow, R. Xu, *medRxiv* preprint 2022, 10.1101/2022.02.21.22271300.

[3] G. Ritchie, D. J. Harvey, F. Feldmann, U. Stroeher, H. Feldmann, L. Royle, R. A. Dwek, P. M. Rudd, *Virology* 2010, *399*, 257–269.

[4] H. Chawla, E. Fadda, M. Crispin, *Curr. Opin. Struct. Biol.* 2022, *75*, 102402.

[5] L. Casalino, Z. Gaieb, J. A. Goldsmith, C. K. Hjorth, A. C. Dommer, A. M. Harbison, C. A. Fogarty, E. P. Barros, B. C. Taylor, J. S. McLellan, E. Fadda, R. E. Amaro, *ACS Cent. Sci.* 2020, *6*, 1722–1734.

[6] A. M. Harbison, C. A. Fogarty, T. K. Phung, A. Satheesan, B. L. Schulz, E. Fadda, *Chem. Sci.* 2022, *13*, 386–395.

[7] Y. Watanabe, J. D. Allen, D. Wrapp, J. S. McLellan, M. Crispin, *Science* 2020, *369*, 330–333.

[8] X. Zhao, H. Chen, H. Wang, *Front. Mol. Biosci.* 2021, *8*, 629873.

[9] A. Shajahan, N. T. Supekar, A. S. Gleinich, P. Azadi, *Glycobiology* 2020, *30*, 981–988.

[10] M. Hoffmann, H. Kleine-Weber, S. Schroeder, N. Kruger, T. Herrler, S. Erichsen, T. S. Schiergens, G. Herrler, N. H. Wu, A. Nitsche, M. A. Muller, C. Drosten, S. Pohlmann, *Cell* 2020, *181*, 271–280 e278.

[11] E. Keyaerts, L. Vijgen, C. Pannecouque, E. Van Damme, W. Peumans, H. Egberink, J. Balzarini, M. Van Ranst, *Antiviral Res.* 2007, *75*, 179–187.

[12] M. Stravalaci, I. Pagani, E. M. Paraboschi, M. Pedotti, A. Doni, F. Scavello, S. N. Mapelli, M. Sironi, C. Perucchini, L. Varani, M. Matkovic, A. Cavalli, D. Cesana, P. Gallina, N. Pedemonte, V. Capurro, N. Clementi, N. Mancini, P. Invernizzi, R. Bayarri-Olmos, P. Garred, R. Rappuoli, S. Duga, B. Bottazzi, M. Uguccioni, R. Asselta, E. Vicenzi, A. Matovani, C. Garlanda, *Nat. Immunol.* 2022, *23*, 275–286.

[13] D. Hoffmann, S. Mereiter, Y. Jin Oh, V. Monteil, E. Elder, R. Zhu, D. Canena, L. Hain, E. Laurent, C. Grunwald-Gruber, M. Klausberger, G. Jonsson, M. J. Kellner, M. Novatchkova, M. Ticevic, A. Chabloz, G.

ChemBioChem

Research Article
doi.org/10.1002/cbic.202200463

**Chemistry
Europe**

European Chemical
Societies Publishing

Wirnsberger, A. Hagelkruys, F. Altmann, L. Mach, J. Stadlmann, C. Oostenbrink, A. Mirazimi, P. Hinterdorfer, J. M. Penninger, *EMBO J.* **2021**, *40*, e108375.

[14] V. Rathnavelu, N. B. Alitheen, S. Sohila, S. Kanagesan, R. Ramesh, *Biomed. Rep.* **2016**, *5*, 283–288.

[15] L. C. de Lencastre Novaes, A. F. Jozala, A. M. Lopes, V. de Carvalho Santos-Ebinuma, P. G. Mazzola, A. Pessoa Junior, *Biotechnol. Prog.* **2016**, *32*, 5–13.

[16] P. Gross, H. Seelert, P. Meiser, R. Müller, *J. Pharm. Biomed. Anal.* **2020**, *181*, 113075.

[17] S. Sagar, A. K. Rathinavel, W. E. Lutz, L. R. Struble, S. Khurana, A. T. Schnaubelt, N. K. Mishra, C. Guda, N. Y. Palermo, M. J. Broadhurst, T. Hoffmann, K. W. Bayles, S. P. M. Reid, G. E. O. Borgstahl, P. Radhak-rishnan, *Clin. Transl. Med.* **2021**, *11*, e281.

[18] M. Azarkan, G. Feller, J. Vandenameele, R. Herman, R. El Mahyaoui, E. Sauvage, A. Vanden Broeck, A. Matagne, P. Charlier, F. Kerff, *Sci. Rep.* **2018**, *8*, 11508.

[19] E. J. M. V. Damme, W. J. Peumans, A. Barre, P. Rougé, *Crit. Rev. Plant Sci.* **1998**, *17*, 575–692.

[20] M. D. Swanson, H. C. Winter, I. J. Goldstein, D. M. Markovitz, *J. Biol. Chem.* **2010**, *285*, 8646–8655.

[21] M. D. Swanson, D. M. Boudreaux, L. Salmon, J. Chugh, H. C. Winter, J. L. Meagher, S. Andre, P. V. Murphy, S. Oscarson, R. Roy, S. King, M. H. Kaplan, I. J. Goldstein, E. B. Tarbet, B. L. Hurst, D. F. Smee, C. de la Fuente, H. H. Hoffmann, Y. Xue, C. M. Rice, D. Schols, J. V. Garcia, J. A. Stuckey, H. J. Gabius, H. M. Al-Hashimi, D. M. Markovitz, *Cell* **2015**, *163*, 746–758.

[22] O. Blixt, S. Head, T. Mondala, C. Scanlan, M. E. Huflejt, R. Alvarez, M. C. Bryan, F. Fazio, D. Calarese, J. Stevens, N. Razi, D. J. Stevens, J. J. Skehel, I. van Die, D. R. Burton, I. A. Wilson, R. Cummings, N. Bovin, C. H. Wong, J. C. Paulson, *Proc. Nat. Acad. Sci.* **2004**, *101*, 17033–17038.

[23] S. Olivera-Ardid, N. Khasbiullina, A. Nokel, A. Formanovsky, I. Popova, T. Tyrtysh, R. Kunetskiy, N. Shilova, N. Bovin, D. Bello-Gil, R. Mañez, *J. Vis. Exp.* **2019**, e57662.

[24] N. Fornstedt, J. Porath, *FEBS Lett.* **1975**, *57*, 5.

[25] M. N. Lund, C. A. Ray, *J. Agric. Food Chem.* **2017**, *65*, 4537–4552.

[26] O. Oyelaran, J. C. Gildersleeve, *Curr. Opin. Chem. Biol.* **2009**, *13*, 406–413.

[27] S. Perez, A. Sarkar, A. Rivet, C. Breton, A. Imberty, *Methods Mol. Biol.* **2015**, *1273*, 241–258.

[28] O. C. Grant, H. M. Smith, D. Firsova, E. Fadda, R. J. Woods, *Glycobiology* **2014**, *24*, 17–25.

[29] I. Joachim, S. Rikker, D. Hauck, D. Ponader, S. Boden, R. Sommer, L. Hartmann, A. Titz, *Org. Biomol. Chem.* **2016**, *14*, 7933–7948.

[30] a) R. Sommer, S. Wagner, A. Varrot, C. M. Nycholat, A. Khaledi, S. Häussler, J. C. Paulson, A. Imberty, A. Titz, *Chem. Sci.* **2016**, *7*, 4990–5001; b) D. Hauck, I. Joachim, B. Frommeyer, A. Varrot, B. Philipp, H. M. Möller, A. Imberty, T. E. Exner, A. Titz, *ACS Chem. Biol.* **2013**, *8*, 1775–1784.

[31] a) G. Beshr, A. Sikandar, E.-M. Jemiller, N. Klymiuk, D. Hauck, S. Wagner, E. Wolf, J. Koehnke, A. Titz, *J. Biol. Chem.* **2017**, *292*, 19935–19951; b) G. Beshr, R. Sommer, D. Hauck, D. C. B. Siebert, A. Hofmann, A. Imberty, A. Titz, *Med. Chem. Commun.* **2016**, *7*, 519–530..

[32] A. C. Walls, Y. J. Park, M. A. Tortorici, A. Wall, A. T. McGuire, D. Veesler, *Cell* **2020**, *181*, 281–292 e286.

[33] A. Shajahan, S. Archer-Hartmann, N. T. Supekar, A. S. Gleinich, C. Heiss, P. Azadi, *Glycobiology* **2021**, *31*, 410–424.

[34] D. Wrapp, N. Wang, K. S. Corbett, J. A. Goldsmith, C.-L. Hsieh, O. Abiona, B. S. Graham, J. S. McLellan, *Science* **2020**, *367*, 1260–1263.

[35] P. A. Longo, J. M. Kavran, M. S. Kim, D. J. Leahy, *Methods Enzymol.* **2013**, *529*, 227–240.